# Tumbling dynamics of inertial inextensible chains in extensional flow

Christophe Henry, Giorgio Krstulovic, and Jérémie Bec
*Université Côte d'Azur, CNRS, OCA, Laboratoire Lagrange, Bd. de l'Observatoire, Nice, France*

(Received 13 February 2018; revised manuscript received 25 June 2018; published 24 August 2018)

This paper investigates the effect of inertia on the dynamics of elongated chains to go beyond the overdamped case that is often used to study such systems. For that purpose, numerical simulations are performed considering the motion of freely jointed bead-rod chains in an extensional flow in the presence of thermal noise. The coil-stretch transition and the tumbling instability are characterized as a function of three parameters: the Péclet number, the Stokes number, and the chain length. Numerical results show that the coil-stretch transition remains when inertia is present and that it depends nonlinearly on the Stokes and Péclet numbers. Theoretical and numerical analyses also highlight the role of intermediate stable configurations in the dynamics of elongated chains: chains can indeed remain trapped for a certain time in these configurations, especially while undergoing a tumbling event.

DOI: 10.1103/PhysRevE.98.023107

## I. INTRODUCTION

The dynamics of elongated and flexible chains has attracted much attention in the past few years. Elongated chains are indeed found in a wide range of applications, including in the paper-making industry (the dynamics of fibers impacts the properties of paper [1,2]), in DNA and polymer physics (rheology changes in the presence of polymers [3,4] sometimes leading to glasslike transitions [5,6]), or in biological oceanography (with the central role played by plankton such as diatoms which form chainlike colonies [7]). The challenges associated with such complex systems include the description of their dynamics and conformation in complex flows as well as their effect on rheological properties of fluids (see, e.g., reviews [3,8,9]). This has led to renewed attention to the dynamics of complex-shaped objects and especially for flexible fibers [10–13].

In this paper, we focus on the dynamics of freely jointed chains. Recent experimental studies on elastic filaments have revealed a complex nonlinear dynamics characterized by coil-stretch transitions (i.e., the shift from extended to folded conformations), tumbling and buckling instabilities in various model flows (purely extensional [14,15], or simple shear [16]), as well as with a more complex dynamics (random or chaotic flows [17,18], in the presence of an obstacle [19] or in a microchannel [20]). These experimental findings on the dynamics of chains have been further confirmed through numerous theoretical and numerical studies (see, e.g., [3,9,21–23], and references therein). In particular, simulations based on the slender-body theory have been used to characterize finely the coil-stretch transition and tumbling statistics [9,24] in the case of inertialess fibers. Other simulations of flexible chains using a trumbbell model [25], again in the absence of inertia, have shown that tumbling occurs even in stretching-dominated flow. A recent numerical study based on bead-spring chains has recently shown that fibers are trapped in either coiled or stretched states in the limit of infinite chain sizes and small-enough diffusion [26] in linear and nonlinear extensional flows. Yet, it remains to be seen whether such conclusions remain valid when inertial effects are taken into account while considering an inextensible chain.

Following these recent studies, the aim of the present study is to characterize the effect of inertia on the dynamics of freely jointed chains immersed in an extensional flow with stochastic noise. Particular attention will be paid to both the coil-stretch (CS) transition and the tumbling instability of such chains as well as to characterizing the stable configurations of such chains in such a flow. We consider the case of freely jointed bead-rod chains, i.e., a chain of elementary beads connected by rigid inextensible rods. This model is thus similar to the so-called Kramers chains [27,28]. We introduce a high-order numerical method to impose the inextensibility constraints (also referred to as holonomic constraint in mechanics) in the presence of a stochastic term.

For that purpose, the dynamics of inertial chains in a flow is presented in Sec. II: it provides details on the model used for bead-rod chains (see Sec. II A) together with a theoretical analysis of the stationary states (in Sec. II B) as well as details on the numerical implementation used (see Sec. II C). Then, numerical results are analyzed first for the coil-stretch transition in Sec. III and then for chain tumbling in Sec. IV.

## II. MODEL AND THEORETICAL ANALYSIS

### A. Dynamics of inertial chains

#### 1. Equation of motion for inertial chains

*a. Generic case.* We consider a suspension of inertial, freely jointed chains embedded in an ambient flow and experiencing a viscous drag. Each chain is represented as a bead-rod Kramers chain [27,28], i.e., constituted of $N+1$ beads connected by $N$ rigid inextensible bonds. Each bead labeled $i$ has a given position denoted by $\boldsymbol{X}_i$ and is maintained at a fixed distance $\ell_{\mathrm{K}}$ from consecutive beads in the chain (corresponding to the Kuhn length). Each bead can undergo a free angular motion relative to its neighbors while remaining at a fixed distance $\ell_{\mathrm{K}}$ from them (see Fig. 1). We have further assumed that all beads are identical with a given mass $m$ while neglecting shielding effects (the effect of hydrodynamic interactions is out of the scope of this paper and will be investigated in future studies). Following Newton's second law,

 

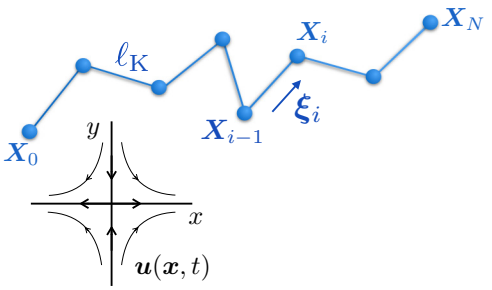


FIG. 1. An elongated chain is approximated as a bead-rod Kramers chain. The beads $\boldsymbol{X}_i$'s are linked together by infinitesimal rigid rods of length $\ell_K$. The orientation of the links is given by the unitary vectors $\boldsymbol{\xi}_i = (\boldsymbol{X}_i - \boldsymbol{X}_{i-1})/\ell_K$.

the individual motion of each bead reads

$$m\frac{d^2\boldsymbol{X}_i}{dt^2} = -\zeta\left[\frac{d\boldsymbol{X}_i}{dt} - \boldsymbol{u}(\boldsymbol{X}_i,t)\right] + \sqrt{2k_BT\,\zeta}\,\boldsymbol{\eta}_i + \lambda_i\,(\boldsymbol{X}_i - \boldsymbol{X}_{i-1}) - \lambda_{i+1}\,(\boldsymbol{X}_{i+1} - \boldsymbol{X}_i), \quad (1)$$

The first term on the right-hand side (RHS) corresponds to the Stokes drag of the beads with a prescribed velocity field $\boldsymbol{u}$ and $\zeta$ denotes the individual drag coefficient of the particles. The second term on the RHS stands for the effect of thermal fluctuations on each bead: $\boldsymbol{\eta}_i$ are independent isotropic white noises, with $T$ denoting the fluid absolute temperature and $k_B$ the Boltzmann constant. The third and fourth terms on the RHS account for the tension (or internal forces) within a chain: $\lambda_i$ is thus the tension between the $i$th and the $(i-1)$th beads. Unlike spring-bead models where the tension is given by a spring force (such as Hookean spring as in [29]), the tensions are here time-dependent Lagrange multipliers associated to the inextensibility constraint $|\boldsymbol{X}_i - \boldsymbol{X}_{i-1}| = \ell_K$ (also referred to as the holonomic constraint in the field of mechanics). This implies that

$$\frac{d}{dt}|\boldsymbol{X}_i - \boldsymbol{X}_{i-1}|^2 = \frac{d^2}{dt^2}|\boldsymbol{X}_i - \boldsymbol{X}_{i-1}|^2 = 0. \quad (2)$$

Using Eq. (1), the tensions satisfy the system

$$0 = [\boldsymbol{X}_i - \boldsymbol{X}_{i-1}]\cdot\{\zeta[\boldsymbol{u}(\boldsymbol{X}_i,t) - \boldsymbol{u}(\boldsymbol{X}_{i-1},t)] + \sqrt{2k_BT\,\zeta}\,[\boldsymbol{\eta}_i - \boldsymbol{\eta}_{i-1}] + 2\lambda_i\,(\boldsymbol{X}_i - \boldsymbol{X}_{i-1}) - \lambda_{i+1}\,(\boldsymbol{X}_{i+1} - \boldsymbol{X}_i) - \lambda_{i-1}\,(\boldsymbol{X}_{i-1} - \boldsymbol{X}_{i-2})\} + \left|\frac{d(\boldsymbol{X}_i - \boldsymbol{X}_{i-1})}{dt}\right|^2. \quad (3)$$

*b. Small chains in an extensional flow.* In the following, we consider that the chain length is below the smallest scale of variation of the fluid velocity field $\boldsymbol{u}$. In that case, the flow stretching is uniform along the chain since all beads feel the same value $\nabla\boldsymbol{u}$ of the fluid gradient. It is then more natural to reformulate the dynamics in terms of the link unitary directions $\boldsymbol{\xi}_i = (\boldsymbol{X}_i - \boldsymbol{X}_{i-1})/\ell_K$, that is,

$$\frac{d^2\boldsymbol{\xi}_i}{dt^2} = -\frac{\zeta}{m}\left[\frac{d\boldsymbol{\xi}_i}{dt} - \boldsymbol{\xi}_i\cdot\nabla\boldsymbol{u}\right] + 2\lambda_i\,\boldsymbol{\xi}_i - \lambda_{i+1}\,\boldsymbol{\xi}_{i+1} - \lambda_{i-1}\,\boldsymbol{\xi}_{i-1} + \sqrt{\frac{2k_BT\,\zeta}{m^2\ell_K^2}}\,(\boldsymbol{\eta}_i - \boldsymbol{\eta}_{i-1}). \quad (4)$$

The $\lambda_i$'s are again Lagrangian multipliers associated to the inextensibility constraint (constant distance $\ell_K$ between beads), this time reading $|\boldsymbol{\xi}_i| = 1$. Note that neither thermal fluctuations nor inertial effects are neglected: we aim indeed at studying chain sizes that span both the colloidal range (where Brownian motion is predominant) and the inertial range.

We further assume that the fluid gradient is given by the simple case of a 2D extensional flow: The fluid is stretching in the horizontal direction $x$ while it is compressing in the vertical direction $y$ (see also Fig. 1). The velocity gradient then simplifies to

$$\nabla\boldsymbol{u} = \begin{pmatrix}\sigma & 0\\ 0 & -\sigma\end{pmatrix}, \quad (5)$$

where $\sigma > 0$ denotes the local fluid velocity shear rate.

#### 2. Dimensionless parameters

With the assumption that $\nabla\boldsymbol{u}$ depends on a single timescale $\tau_{\text{fluid}} = \sigma^{-1}$, the problem depends upon three dimensionless parameters: the Stokes number St, the Péclet number Pe, and the chain length $N$. First, the *Stokes number* is the ratio between the beads response time and the fluid flow timescale:

$$\text{St} = \frac{\tau_{\text{beads}}}{\tau_{\text{fluid}}} = \frac{\sigma\,m}{\zeta}. \quad (6)$$

It measures the inertia of chains: $\text{St} \ll 1$ corresponds to the case of tracers (i.e., particles following the streamlines) while $\text{St} \gg 1$ designates particles that depart from the fluid streamlines. Second, the *Péclet number* is given by the ratio between the diffusion and the advection timescales:

$$\text{Pe} = \frac{\tau_{\text{diff}}}{\tau_{\text{fluid}}} = \frac{\sigma\,\ell_K^2\,\zeta}{k_BT}. \quad (7)$$

It measures the relative importance between thermal fluctuations and fluid stretching: $\text{Pe} \ll 1$ signifies that thermal fluctuations dominate the dynamics while $\text{Pe} \gg 1$ implies that the dynamics is governed by fluid stretching. It is similar to the Weissenberg number usually used in polymer physics (which measures the ratio between the fluid strain and the diffusion). Third, the *chain length* corresponds to the number of Kuhn links forming the chain:

$$N = \frac{L}{\ell_K}, \quad (8)$$

where $L$ denotes the total length of the chain. It is a measure of the number of degrees of freedom in the chain.

#### 3. Overdamped limit

When the relaxation time of a bead $\tau_{\text{beads}} = m/\zeta$ is much shorter than the fluid flow timescale, the inertial term in Eq. (4) can be neglected. In this overdamped case, the equation

simplifies to

$$\frac{d\boldsymbol{\xi}_i}{dt} = \boldsymbol{\xi}_i \cdot \boldsymbol{\nabla u} + \sqrt{\frac{2k_B T}{\ell_K^2\,\zeta}}\,(\boldsymbol{\eta}_i - \boldsymbol{\eta}_{i-1}) + 2\lambda'_i\,\boldsymbol{\xi}_i - \lambda'_{i+1}\,\boldsymbol{\xi}_{i+1} - \lambda'_{i-1}\,\boldsymbol{\xi}_{i-1}, \tag{9}$$

with $\lambda'$ the renormalized Lagrange multipliers given by $\lambda' = \lambda\, m/\zeta$. As in the inertial case, the tension forces are calculated by imposing a constant distance between consecutive beads which gives the following matrix equation:

$$\boldsymbol{\xi}_i \cdot \frac{d\boldsymbol{\xi}_i}{dt} = 0. \tag{10}$$

In the presence of stochastic forces, both systems [Eqs. (3) and (10)], need to be solved using high-order methods to avoid systematic numerical errors on the distance between beads (details on the numerical implementation are provided in Sec. II C and in the Appendix).

#### *4. Observables*

Since we are interested in the stretching and orientation of freely jointed chains, two observables have been retained to monitor their dynamics in an extensional flow based on the usual parameters measured for fibers and elongated particles [9] as well as on an analogy with spin systems: the chain end-to-end length (analogous to magnetization in spin systems) and the chain orientation (analogous to magnetic energy in spin systems).

First, the chain coarse end-to-end length along the stretching direction is defined as

$$\mathcal{L}(t) = \frac{1}{N}\sum_{i=1}^{N} \operatorname{sgn} \xi_i^x(t). \tag{11}$$

Note that we are using here the sign of segments along the $x$ direction to obtain an end-to-end length equal to $\pm 1$ when the chain is close to being fully stretched.

Second, the chain coarse orientation along the stretching direction is defined as

$$\mathcal{F}(t) = \frac{1}{N-1}\sum_{i=1}^{N-1} \operatorname{sgn} \xi_i^x(t) \operatorname{sgn} \xi_{i+1}^x(t). \tag{12}$$

It measures the relative orientation of consecutive beads in the chain.

In the following, we characterize the evolution of chains in terms of theses two quantities and as a function of the three parameters of the system: the chain length (number of links) $N$, the Péclet number Pe, and the Stokes number St.

### B. Stationary states

In the absence of noise, all configurations where the unitary link vectors $\boldsymbol{\xi}_i$ are aligned with the stretching direction $x$ are steady solutions to Eq. (4). Indeed, if we assume that $\boldsymbol{\xi}_i = (\varepsilon_i, 0)^{\mathsf{T}}$ with $\varepsilon_i = \pm 1$, the dynamics is trivially stationary if the tensions satisfy

$$-2\varepsilon_i\,\lambda_i + \varepsilon_{i+1}\,\lambda_{i+1} + \varepsilon_{i-1}\,\lambda_{i-1} = \frac{\zeta\,\sigma}{m}\,\varepsilon_i. \tag{13}$$

This system always admits solutions of the form $(\lambda_1, \ldots, \lambda_N)^{\mathsf{T}} = (\zeta\,\sigma/m)\,\mathbb{E}^{-1}\,(\varepsilon_1, \ldots, \varepsilon_N)^{\mathsf{T}}$, where $\mathbb{E}$ denotes the tridiagonal matrix with elements $\mathbb{E}_{i,j} = \varepsilon_{i+1}\delta_{i+1,j} - 2\varepsilon_i\delta_{i,j} + \varepsilon_{i-1}\delta_{i-1,j}$ and whose determinant reads $\det \mathbb{E} = (-1)^N\,(N+1)\,\varepsilon_1 \cdots \varepsilon_N \neq 0$. These stationary configurations comprise the case of a fully stretched chain for which $\varepsilon_i = +1$ for all $i$, as well as the alternating folded polymer associated to $\varepsilon_i = (-1)^i$. Besides these extremes, other intermediate configurations are allowed corresponding to partial folding of the chain.

If such stationary configurations are stable, they could play an important role in the dynamics. For instance, the system could, in the presence of noise, spend some time in those states. To evaluate the linear stability of these various cases, let us consider that the link vectors are of the form $\boldsymbol{\xi}_i = (\varepsilon_i \sqrt{1-\alpha_i^2}, \alpha_i)^{\mathsf{T}}$ with $\alpha_i \ll 1$. Clearly, the perturbation of the stationary state is order $\alpha^2$ in the $x$ direction, as well as for the tension equation (13). The dominant evolution is thus in the $y$ direction and reads

$$\frac{d^2\alpha_i}{dt^2} = -\frac{\zeta}{m}\left[\frac{d\alpha_i}{dt} + \sigma\alpha_i\right] + 2\lambda_i\alpha_i - \lambda_{i+1}\alpha_{i+1} - \lambda_{i-1}\alpha_{i-1},$$

which can be written in vectorial form as

$$\frac{d}{dt}\begin{pmatrix}\boldsymbol{\alpha}\\ \dot{\boldsymbol{\alpha}}\end{pmatrix} = \mathcal{M}\begin{pmatrix}\boldsymbol{\alpha}\\ \dot{\boldsymbol{\alpha}}\end{pmatrix},$$

$$\text{with}\quad \mathcal{M} = \begin{pmatrix}\mathbb{O}_N & \mathbb{I}_N\\ -[(\zeta\,\sigma/m)\,\mathbb{I}_N + \boldsymbol{\Delta}_\lambda] & -(\zeta/m)\,\mathbb{I}_N\end{pmatrix}. \tag{14}$$

$\mathbb{O}_N$ and $\mathbb{I}_N$ denote the $N \times N$ zero and identity matrices, respectively. We have introduced $\boldsymbol{\alpha} = (\alpha_1, \ldots, \alpha_N)^{\mathsf{T}}$, $\dot{\boldsymbol{\alpha}} = (d\alpha_1/dt, \ldots, d\alpha_N/dt)^{\mathsf{T}}$, and $\boldsymbol{\Delta}_\lambda$ the tridiagonal matrix with elements $(\Delta_\lambda)_{i,j} = \lambda_{i+1}\delta_{i+1,j} - 2\lambda_i\delta_{i,j} + \lambda_{i-1}\delta_{i-1,j}$.

The linear stability of stationary configurations is entailed in the eigenvalue $\mu_{\mathcal{M}}$ of the matrix $\mathcal{M}$ which has the largest real part. One can easily check that for all stationary configurations obeying (13), the vector $\boldsymbol{\alpha} = (\varepsilon_1, \ldots, \varepsilon_N)^{\mathsf{T}}$ and $\dot{\boldsymbol{\alpha}} = \mu\,\boldsymbol{\alpha}$ is an eigenvector associated to the eigenvalue $\mu$ if the latter satisfies $\mu^2 + (\zeta/m)\,\mu + 2\,\zeta\,\sigma/m = 0$. We thus obtain the following lower bound:

$$\operatorname{Re}(\mu_{\mathcal{M}}) \geqslant \frac{\sigma}{2\,\mathrm{St}}\operatorname{Re}[\sqrt{1-8\,\mathrm{St}} - 1]. \tag{15}$$

The right-hand side has a nonmonotonic behavior as a function of the Stokes number St. We can thus expect some stationary states to get stabilized by a moderate inertia. However, these states necessarily become less stable when $\mathrm{St} \to \infty$. This is illustrated below.

#### *1. The stretched line*

Let us first consider the stationary state where all rods are aligned with the stretching direction, i.e., $\varepsilon_i = \varepsilon$ for all $i$, with $\varepsilon = \pm 1$. Equation (13) becomes

$$-2\lambda_i + \lambda_{i+1} + \lambda_{i-1} = \zeta\sigma/m \quad \text{with } \lambda_0 = \lambda_{N+1} = 0,$$

so that the tensions read

$$\lambda_i = -[\zeta\sigma/(2m)]i(N+1-i). \tag{16}$$

As can be seen from Fig. 2, this configuration is always stable, independently of the Stokes number and the number $N$ of Kuhn

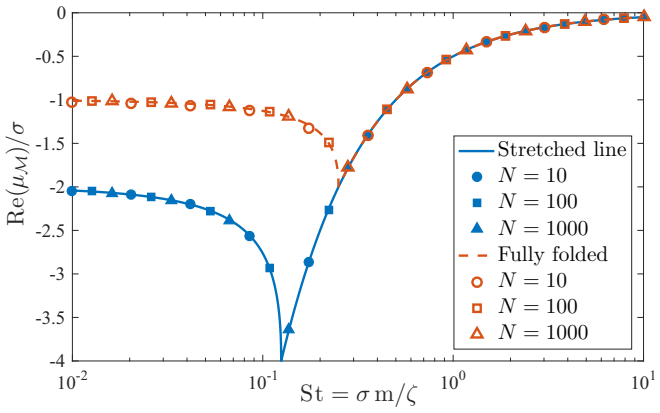


FIG. 2. Real part of the most unstable eigenvalue $\mu_{\mathcal{M}}$ (in units of the fluid shear rate $\sigma$) as a function of the Stokes number St for the fully stretched chain (solid line, filled symbol) and the completely folded case (dashed line, empty symbols). The lines show the predictions (see text), while symbols are numerical evaluations for various chain lengths, as labeled.

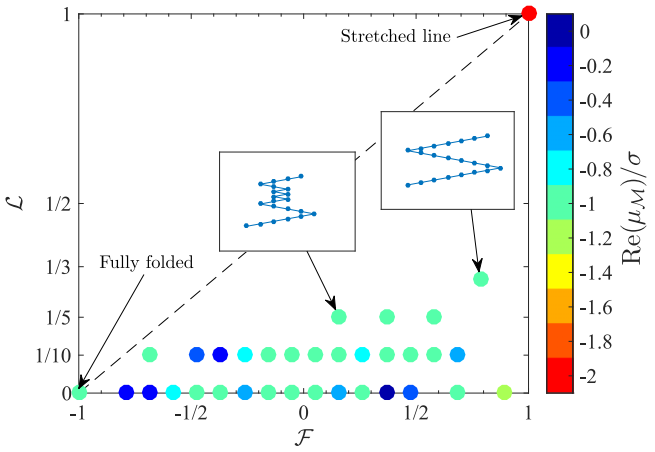


FIG. 3. Stable configurations of a chain with $N = 20$ and $\mathrm{St} = 0$ in the $(\mathcal{F}, \mathcal{L})$ plane. The filled circles stand for the real part of the less stable eigenvalue $\mu_{\mathcal{M}}$ (in units of $\sigma$). Two intermediate stable configurations are singled out at $\mathcal{L} \approx 1/3$, $\mathcal{F} = (N-5)/(N-1)$, where the chain is approximately folded in three equal pieces, and at $\mathcal{L} = 1/5$ and $\mathcal{F} \approx 0.15$, for which the chain alternates between stretched and folded segments.

lengths in the chain. In addition, the less stable eigenvalue $\mu_{\mathrm{M}}$ is exactly equal in that case to the lower bound (15) discussed above. Inertia tends to stabilize this configuration up to $\mathrm{St} = 1/8$. Above this value, the stretched line becomes less stable with $\mathrm{Re}\,(\mu_{\mathcal{M}}) = \sigma/(2\,\mathrm{St})$.

#### 2. Folded polymer

A second stationary configuration of interest is the case when the chain is completely folded in an accordion shape. We have in that case $\varepsilon_i = (-1)^i$, so that the equations for the tensions become

$$2\lambda_i + \lambda_{i+1} + \lambda_{i-1} = -\zeta\sigma/m, \tag{17}$$

which yields

$$\lambda_i = -\frac{\zeta\sigma}{4m}[1-(-1)^i] - \frac{\zeta\sigma}{4m}\frac{i(-1)^i}{N+1}[1+(-1)^N]. \tag{18}$$

This time, the associated matrix $\mathbf{\Delta}_\lambda$ admits zero modes. Indeed, if without loss of generality we assume that $N$ is odd, the second term in the right-hand side of (18) vanishes and the $\lambda_i$ alternate between $-\zeta\sigma/(2m)$ and 0. Any vector $\boldsymbol{\alpha}$ with vanishing odd components belongs to the kernel of $\mathbf{\Delta}_\lambda$. As a consequence, vectors of the form $(\boldsymbol{\alpha}, \mu\boldsymbol{\alpha})$ are eigenvectors of $\mathcal{M}$ associated to the eigenvalue

$$\mu = \frac{\sigma}{2\,\mathrm{St}}[\sqrt{1-4\,\mathrm{St}} - 1].$$

As can be seen in Fig. 2, such eigenvalues correspond to the less stable mode of this stationary configuration. As for the stretched line, a sufficiently small inertia has a stabilizing effect. The critical value is this time $1/4$, so that when $\mathrm{St} > 1/4$, the configuration in accordion shape is as stable as the fully stretched chain.

#### 3. Intermediate configurations

Besides these two extreme configurations, there exists in general a large number of possible stationary states, as illustrated in Fig. 3 in the overdamped ($\mathrm{St} = 0$) case for $N = 20$. These various configurations were obtained numerically by a Monte Carlo method. The fully stretched line (in the top-right corner) is in that case the most stable configuration with $\mathrm{Re}\,(\mu_{\mathcal{M}}) = -2\sigma$. The fully folded accordion shape in the bottom-left corner is associated to $\mathrm{Re}\,(\mu_{\mathcal{M}}) = -\sigma$. Other stable configurations associated to partial foldings of the chain span the bottom half of the $(\mathcal{F}, \mathcal{L})$ plane. We expect the fiber to explore them in the presence of noise. This will be the case during the tumbling of the chain, as we will see later in Sec. IV.

### C. Numerical implementation

In the presence of noise, we simulate the dynamics of chains by integrating numerically their equation of motion given by Eq. (4). To that extent, we resort to an explicit first-order Euler-Maruyama method with temporal discretization. In that case, the discretized system reads:

$$\begin{aligned}\boldsymbol{V}_i(t+\Delta t) = \boldsymbol{V}_i(t) &+ \Delta t\{-(\zeta/m)[\boldsymbol{V}_i(t) - \boldsymbol{\xi}_i(t)\cdot\boldsymbol{\nabla u}] \\ &+ 2\lambda_i\boldsymbol{\xi}_i(t) - \lambda_{i+1}\boldsymbol{\xi}_{i+1}(t) - \lambda_{i-1}\boldsymbol{\xi}_{i-1}(t)\} \\ &+ \sqrt{\frac{2k_{\mathrm{B}}T\zeta}{m^2\ell_{\mathrm{K}}^2}}\,(\Delta\boldsymbol{W}_i - \Delta\boldsymbol{W}_{i-1}), \\ \boldsymbol{\xi}_i(t+\Delta t) = \boldsymbol{\xi}_i(t) &+ \Delta t\boldsymbol{V}_i(t),\end{aligned} \tag{19}$$

where $\boldsymbol{\xi}_i$ is the segment labeled "$i$" and $\boldsymbol{V}_i = d\boldsymbol{\xi}_i/dt$ its velocity, $\Delta t$ is the time step used in the simulation, and $\Delta\boldsymbol{W}_i$ are the increments of a two-dimensional Wiener process over a time step $\Delta t$.

To close the system given by Eq. (19), the inextensibility constraint (or holonomic constraint) $|\boldsymbol{\xi}_i(t+\Delta t)|^2 = |\boldsymbol{\xi}_i(t)|^2$ is used to evaluate the tensions $\lambda_i$. Replacing with the discretized system, this constraint reads

$$2\boldsymbol{\xi}_i(t)\cdot\boldsymbol{V}_i(t) + \Delta t|\boldsymbol{V}_i(t)|^2 = 0. \tag{20}$$

This matrix equation depends nonlinearly on $\boldsymbol{\xi}_i(t)$ and $\lambda_i$. As a result, there is no easy numerical resolution of the tensions $\lambda_i$.

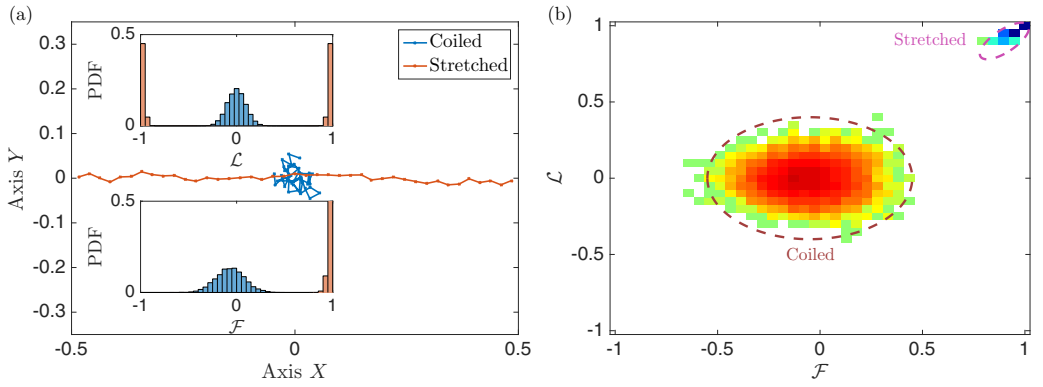


FIG. 4. End-to-end length and orientation of a freely jointed chain ($N = 40$) at two values of Péclet numbers showing the chain in both the coiled state (Pe = 0.05) and the stretched state (Pe = 0.3). (a) Snapshots of a chain in the coiled and stretched states. The insets display the histograms of $\mathcal{L}$ and $\mathcal{F}$ for both states. (b) Map showing the probability of occurrence for each discrete state in the $(\mathcal{F}, \mathcal{L})$ plane around the coiled (hot color) and stretched state (cold color).

However, we note that tension forces have the same scaling as the stochastic term and it can be written as a series expansion in powers of $(\Delta t)^{1/2}$. This provides a new high-order method for the numerical simulation of bead-rod chains (further details are given in the Appendix).

## III. COILED-STRETCHED TRANSITION

### A. Principle and mechanism

Chain orientation changes constantly due to the competition between fluid stretching and thermal fluctuations. As a result, they explore a wide range of states, leading to a broad distribution in the end-to-end length and orientation (see Fig. 4). In particular, two notable states can be reached, corresponding to a stretched and a coiled configuration, respectively, and that are typical of flexible particles such as fibers or polymers. These two states have been studied for a long time in the field of polymer science [4,30] and have recently attracted more studies in the multiphase flow community [3,9].

Similarly to the well-studied conformation of polymers [4], chains are stretched when fluid strain prevails over thermal fluctuations, i.e., Pe $\gg 1$. The probability density function of $\mathcal{L}(t)$ and $\mathcal{F}(t)$ are peaked toward unity (with the end-to-end length being either positive or negative depending on the chain orientation with respect to the fluid). Oppositely, chains are coiled when thermal fluctuations are predominant over fluid stretching, i.e., Pe $\ll 1$. In that case, it is well known that the probability density function (PDF) of $\mathcal{L}(t)$ and $\mathcal{F}(t)$ both display a Gaussian distribution with zero mean due to the random orientation of consecutive links.

Another way to differentiate between coiled and stretched states is to have a look at the chain orientation and end-to-end length in the $(\mathcal{F}, \mathcal{L})$ plane [see Fig. 4(b)]. Chains in the coiled state remain around the configuration $(\mathcal{F}, \mathcal{L}) \sim (0, 0)$, whereas chains in the stretched state are close to $(\mathcal{F}, \mathcal{L}) \sim (1, 1)$. Figure 4(b) also provides additional information on the nearby partially folded or unfolded states that chains explore. These states can be related to the intermediate stable configurations that have been identified in Sec. II B 3. Besides, it appears that the range of nearby states accessible depends on the relative importance of thermal fluctuations to fluid stretching.

The CS transition has been extensively studied in the literature in the overdamped case, i.e., when inertia is negligible (see, for instance, [3,14,25,26,28,30–34]). In the following, we characterize the effect of inertia on the CS transition for such elongated chains using the two observables $(\mathcal{L}, \mathcal{F})$.

### B. Validation of the model: Overdamped case

Before evaluating the effect of inertia on the CS transition, the current model for the dynamics of freely jointed chains is first validated by studying the well-known overdamped case.

For that purpose, we first characterize the chain end-to-end length and orientation as a function of time. Both observables $(\mathcal{L}, \mathcal{F})$ are indeed fluctuating all the time due to instantaneous thermal fluctuations which can change the chain conformation. In line with previous studies on coil-stretch transitions (see, e.g., [3]), we have measured both observables after a fixed time (roughly equal to ten times the transition time from one state to another one, which is a complex function of Pe, St, and $N$).

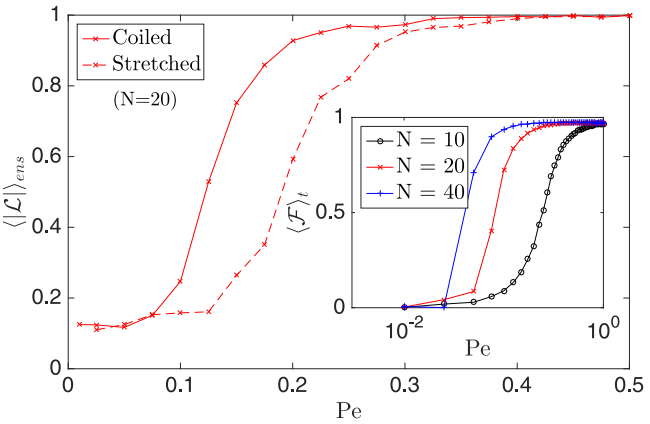


FIG. 5. Chain end-to-end length and orientation as a function of Pe showing the subcritical phase transition for $N = 10$, 20, and 40. Subcritical phase transition visible when plotting the average over several realizations of the flow $\langle|\mathcal{L}|\rangle_{\text{ens}}$. Inset showing the average orientation over time $\langle\mathcal{F}\rangle_t$.

Figure 5 displays the chain end-to-end length averaged over several realizations of the flow $\langle|\mathcal{L}|(t)\rangle_{\rm ens}$ taken after this fixed time. Two main results are retrieved from this figure.

First, the CS transition is related to the balance between thermal fluctuations and fluid stretching: a chain is indeed stretched for high fluid stretching, i.e., Pe $\gtrsim 1$, whereas it is coiled for high fluctuations, i.e., Pe $\ll 1$. The ensemble averaged end-to-end length $\langle|\mathcal{L}|\rangle_{\rm ens}$ is proportional to $1/\sqrt{N}$ at small Péclet number due to the random orientation of consecutive beads when thermal fluctuations are high (the central limit theorem then applies). Second, a conformation hysteresis can be observed, similarly to the hysteresis loop that has been observed for long polymers or DNA molecules in a flow [3]. This hysteresis can be interpreted as resulting from higher internal constraints found in a stretched chain. We have indeed seen in Sec. II B that the tensions behave quadratically in a stretched configuration, while they are at best linear in a coiled chain: this makes it harder to start folding a stretched chain than to start unfolding a coiled chain.

To further assess the effect of Pe on $\mathcal{L}$ and $\mathcal{F}$, the time-averaged chain end-to-end length and orientation has been extracted from numerical simulations when a stationary state is reached. The inset in Fig. 5 displays the orientation $\langle\mathcal{F}\rangle$ as a function of the Péclet number Pe. It confirms that chains are coiled for Pe $\ll 1$ and stretched for Pe $\gtrsim 1$. It also appears that the evolution of $\langle\mathcal{F}\rangle$ with Pe is monotonic: It decreases toward 0 when Pe decreases. It should be noted here that hysteresis is not visible since results have been averaged over time, i.e., the dependence on the initial conditions has been lost in the process.

The CS transition is also affected by the chain length: Fig. 5 shows that the CS transition occurs at smaller values of the Péclet number when the chain length $N$ increases. This is in agreement with recent results [26], where the hysteresis curve was shown to occur at smaller values of the flow strength (the Deborah number in the original article). To further confirm these trends, the chain end-to-end length averaged over time $\langle|\mathcal{L}|\rangle_t$ has been characterized as a function of both $N$ and Pe. Results are plotted in Fig. 6: One observes that a long chain is usually coiled for Pe $\lesssim 0.1$ while it remains stretched for Pe $\gtrsim 0.4$. The transition between the coiled and stretched states can be distinguished using a critical Péclet number Pe$^\star$, defined as the value at which the averaged chain end-to-end length exceeds a certain threshold $\langle|\mathcal{L}|\rangle_t > L^\star$. The solid red line in Fig. 6 displays this critical Péclet number for $L^\star = 0.9$. The CS transition has a nontrivial dependence on the chain length: It becomes independent of the chain length $N$ for sufficiently long chains (here around $N \gtrsim 30$), but it occurs at increasing Péclet numbers with small chains (here $30 \gtrsim N \gtrsim 4$). It should be noted here that, in the case of infinitely long chains, the assumption of a constant gradient along the chain is debatable: it nevertheless provides interesting trends and such effects will be studied in future work by explicitly calculating the dynamics of very long chains in homogeneous isotropic turbulence.

### C. Impact of inertia on the coil-stretch transition

The model having been validated and characterized in the overdamped case, we now focus on assessing the effect of inertia on the coil-stretch transition. To that extent, we

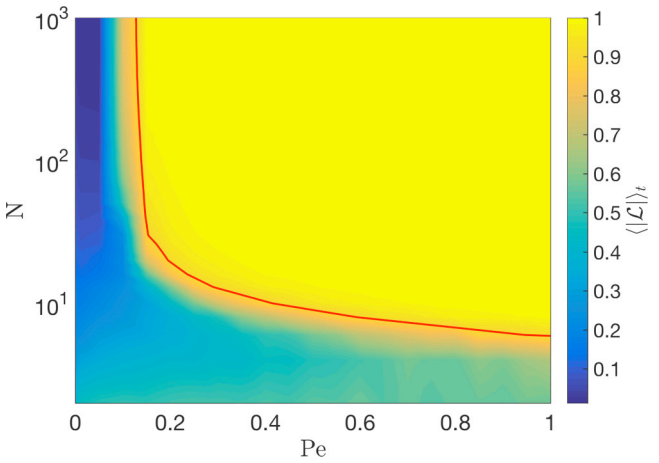


FIG. 6. Average chain end-to-end length over time $\langle\mathcal{L}\rangle_t$ in the (Pe, $N$) plane. The red solid line corresponds to the critical Péclet number Pe$^\star$ at which the chain end-to-end length exceeds a threshold $\langle|\mathcal{L}|\rangle_t > L^\star = 0.9$. This shows the existence of an asymptotic regime for sufficiently long chains.

characterize a chain end-to-end length and orientation as a function of both Pe and St for a given length. Drawing on the observations made in the overdamped case, we have retained a chain length $N = 20$, which is large enough to be representative of the behavior of long chains, but not too large to remain numerically tractable.

The dynamics is impacted by the inertia of each bead. In particular, two regimes can be identified depending on whether the Stokes number is greater or higher than 1/8. Indeed, as was shown in Sec. II B 1 (in the absence of noise), for St $< 1/8$ the eigenvalues of a stretched chain are real [see Eq. (15)]. Therefore, at small Stokes numbers, the inertial dynamics can be seen as that of an overdamped chain in a synthetic compressible flow where the effective compression rate reads $\sigma(1 + 2\,\mathrm{St})$.

Figure 7 shows the time-averaged chain end-to-end length $\langle|\mathcal{L}|\rangle_t$ in the (Pe, St) plane. One clearly observes that for

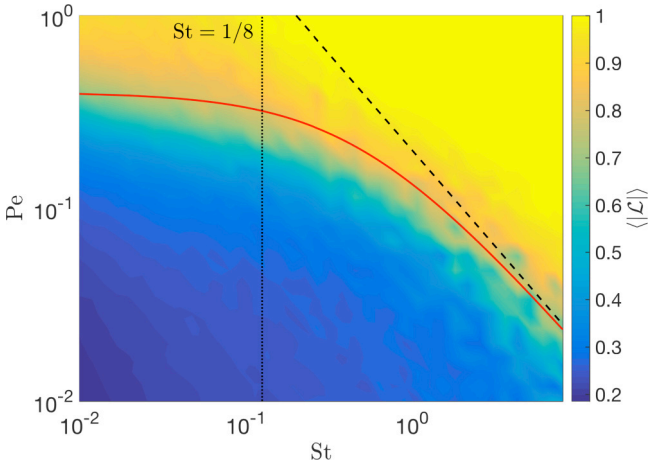


FIG. 7. Time-averaged extension $\langle\mathcal{L}\rangle_t$ in the (St, Pe) plane. The dotted vertical line shows the critical value St $= 1/8$. The solid and dashed lines display the prediction Pe$^\star$(St) $=$ Pe$^\star(0)/(1 + 2\,\mathrm{St})$ and the asymptotic behavior Pe$^\star$(St) $=$ Pe$^\star(0)/(2\,\mathrm{St})$, respectively, with Pe$^\star(0) = 0.4$.

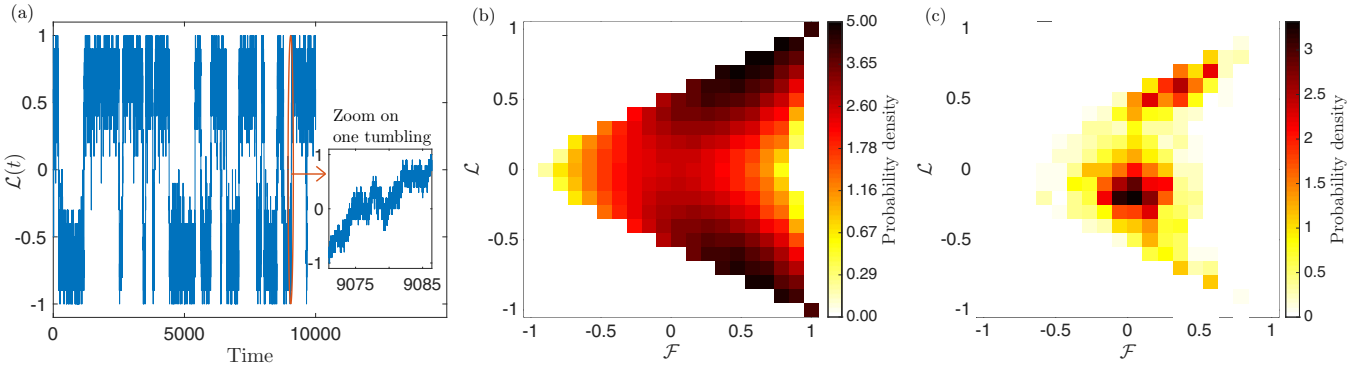


FIG. 8. Evolution of the chain orientation for $N = 20$ near the CS transition (here $\mathrm{Pe} = 0.14$) in the overdamped case. (a) Chain orientation $\mathcal{L}(t)$ as a function of time. Inset showing a zoom on a selected tumbling event. (b) Probability of occurrence for each discrete state over the whole simulation in the $(\mathcal{F}, \mathcal{L})$ plane. (c) Analogous to (b) but over a selected tumbling event.

$St < 1/8$, the CS transition occurs at a critical value of the Péclet number that is compatible with the formula $\mathrm{Pe}^\star(\mathrm{St}) = \mathrm{Pe}^\star(0)/(1 + 2\,\mathrm{St})$ obtained using the effective compression rate described above. Surprisingly, this behavior describes also what is happening for $\mathrm{St} > 1/8$. At very large Stokes numbers, the critical Péclet number decreases as a power law $\mathrm{Pe}^\star(\mathrm{St}) \propto \mathrm{St}^{-1}$. This can be interpreted using dimensional analysis as follows: The CS transition results from the competition between thermal fluctuations and fluid stretching and thus occurs when both contributions are balanced. According to Eq. (4), this means $1/\mathrm{St} \sim 1/(\mathrm{PeSt}^2)$ and thus $\mathrm{Pe} \sim \mathrm{St}^{-1}$.

## IV. TUMBLING

### A. Principle and mechanism

Another typical feature of elongated particles is the existence of tumbling events [25,35–38]. These events correspond to the reversal of the chain orientation with respect to the fluid stretching. This is illustrated in Fig. 8(a): A chain is trapped in one of the stretched configurations with $\mathcal{L} = \pm 1$ for a long time until a sufficiently high fluctuation makes it tumble. The inset of Fig. 8(a) shows a focus on one of the tumbling events: It occurs due to a favorable sequence of thermal fluctuations that allows the chain to transition from a stretched state to a coiled state, before unfolding toward the reversed stretched configuration. This process is thus similar to the tumbling-through-folding motion that has been recently characterized for trumbbells [25] or polymers [36].

Further information on the intermediate states explored during the tumbling event has been obtained by studying the probability of occurrence for each discrete state in the $(\mathcal{F}, \mathcal{L})$ plane. This is displayed in Figs. 8(b) and 8(c), which highlights the signature of intermediate states in tumbling. The chains seem to stay temporarily close to the secondary stable states described in the stability analysis of Sec. II B 3. In the present case, the state where $(\mathcal{F} \approx 0.15, \mathcal{L} \approx -0.2)$ is rather frequent during the tumbling transition. It corresponds to the partially coiled configuration shown in Fig. 3.

In the following, we characterize the tumbling dynamics of inertial chains in terms of the two observables $(\mathcal{L}, \mathcal{F})$.

### B. Validation of the model: Overdamped case

As in the case of the coil-stretch transition, we start by analyzing numerical results in the well-known overdamped case to validate our approach.

We first evaluate the persistence time $\tau_t$, which corresponds to the time spent by a fiber in an extended state. In that sense, $\tau_t$ measures the time separating two tumbling events. As revealed by Fig. 8(a), the persistence time is distributed randomly. Figure 9 displays the PDF of the persistence time for various values of the Péclet number (slightly above the critical Péclet $\mathrm{Pe}^\star$ at which the CS transition occurs). First, it can be seen that the value of the persistence time is high, especially compared to recent experimental data on polymer dynamics in extensional flows which measured a residency time around 6 s for a shear rate of 0.86 $\mathrm{s}^{-1}$ [39]. Second, the PDF turns out to have an exponential tail for large $\tau_t$, i.e., $p(\tau_t) \propto \exp(-\tau_t/\tau_t^{\mathrm{avg}})$ with $\tau_t^{\mathrm{avg}}$ the average persistence time. This exponential tail is in line with recent numerical and theoretical results on tumbling [25].

These recent theoretical results [25] also predict that the mean persistence time increases exponentially when the amplitude of the noise decreases. This relates to the fact that it becomes harder for chains to exit the stretched state when

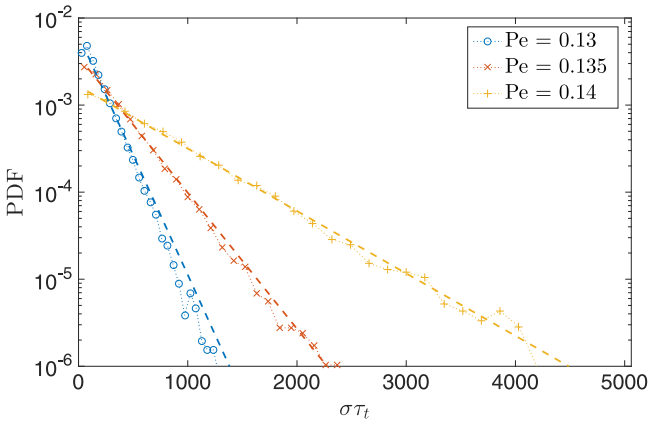


FIG. 9. Probability density function (PDF) of the persistence time for $N = 20$ in the overdamped case for various values of the Péclet number (slightly above the CS transition). The dotted lines correspond to the exponential law $p(\tau_t) = \exp(-\tau_t/\tau_t^{\mathrm{avg}})/\tau_t^{\mathrm{avg}}$.

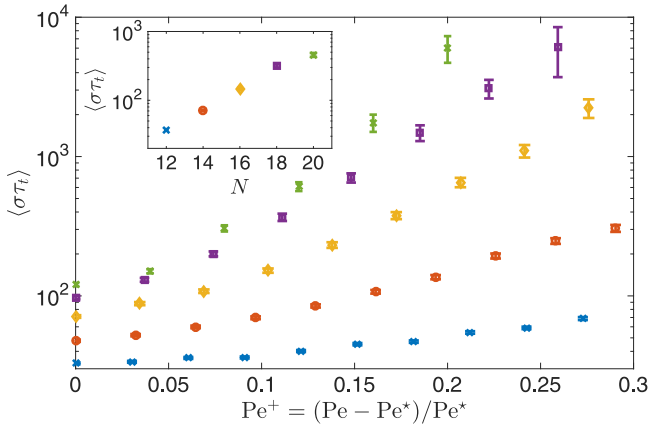


FIG. 10. Average persistence time $\langle \tau_t \rangle$ as a function of the normalized Péclet number $\mathrm{Pe}^+ = (\mathrm{Pe} - \mathrm{Pe}^\star)/\mathrm{Pe}^\star$. Inset showing the evolution of the persistence time $\langle \tau_t \rangle$ with the chain length $N$.

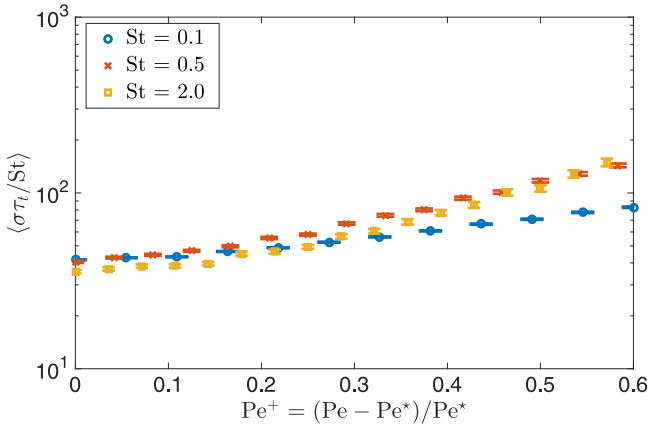


FIG. 11. Average persistence time $\langle \tau_t \rangle$ as a function of the normalized Péclet number $\mathrm{Pe}^+ = (\mathrm{Pe} - \mathrm{Pe}^\star)/\mathrm{Pe}^\star$ for various Stokes number ($N = 20$).

the amplitude of thermal fluctuations decreases. This trend is confirmed in Fig. 10, where the average persistence time is plotted as a function of the reduced Péclet number $\mathrm{Pe}^+ = (\mathrm{Pe} - \mathrm{Pe}^\star)/\mathrm{Pe}^\star$. It also appears that, when fluctuations are small enough (here for $\mathrm{Pe}^+ > 0.1$), there is an exponential increase of $\langle \tau_t \rangle$ with $\mathrm{Pe}^+$. Besides, as seen in the inset of Fig. 10, the persistence time increases very rapidly as a function of the chain length $N$. This means that chains are trapped in either stretched state as $N \to \infty$ and that there is a loss of ergodicity as the chain length diverges at a fixed Péclet number. A similar ergodicity breaking has been reported for the CS transition [26]. This has been explained theoretically by reducing the problem to thermally activated transitions over an energy barrier described by a rate theory. The same applies here: The energy needed for a chain to escape from one attractor (or state) to another is proportional to the chain length. As a result, the transition rate decays exponentially with the chain length $N$.

### C. Impact of inertia on the tumbling dynamics

The model having been validated and characterized in the overdamped case, we now focus on assessing the effect of inertia on the tumbling dynamics. In line with the previous analysis of the CS transition including inertial effects, we have chosen to fix the chain length to $N = 20$ and to assess how the tumbling dynamics evolves with both Péclet and Stokes numbers.

In line with the previous analysis, the mean persistence time is expected to increase exponentially as the amplitude of the noise decreases for a given value of the Stokes number. This is confirmed in Fig. 11 that displays the evolution of the persistence time as a function of the reduced Péclet number $\mathrm{Pe}^+$ for three values of the Stokes number (respectively, 0.1, 0.5, and 2). Besides, it also appears from Fig. 11 that the persistence time increases with the Stokes number. This is in line with recent theoretical results [37] showing a decrease in the tumbling rate for increasing inertia.

Furthermore, two regimes can be identified in Fig. 11: First, close to the CS transition ($\mathrm{Pe}^+ \lesssim 0.1$), the persistence time increases linearly with the Stokes number and all curves collapse on a single master curve when plotting $\tau_t/\mathrm{St}$ as a function of the reduced Péclet number $\mathrm{Pe}^+$. Second, at larger Péclet numbers ($\mathrm{Pe}^+ \gtrsim 0.1$), different behaviors are displayed by the two families of particles. Low-inertia particles ($\mathrm{St} < 1/8$) appear indeed to tumble at a higher rate than high-inertia particles ($\mathrm{St} > 1/8$).

## V. CONCLUDING REMARKS

The dynamics of inertial deformable chains has been explored in the case of an extensional flow. In particular, we have assessed the role of the Péclet number, Stokes number, and chain length on the dynamics of such chains, especially regarding the coil-stretch transition and tumbling phenomena. The current approach has been first validated by comparing numerical results to well-known results on the coil-stretch transition in the overdamped case. Then, the effect of inertia on this transition has been characterized: It was shown that the transition depends nonlinearly on the three parameters and that, for a given chain length, it evolves proportionally to $1/(1 + 2\,\mathrm{St})$. Second, numerical results obtained with the current approach have been compared to well-known results on tumbling dynamics of chains. In particular, the simulations support recent results on the loss of ergodicity as the chain length goes to infinity (meaning that chains are kinetically trapped in a given stretched state). Then, the effect of inertia on the tumbling dynamics of such chains has been characterized: it was shown that the persistence time increases nonlinearly with the Stokes number.

These promising results on the dynamics of inertial chains in an extensional flow call for further refinements and developments. In particular, it is worth assessing how 3D simulations affect these results and to see if recent results showing a higher tendency for trumbbells to remain in the stretched state in 3D cases than in 2D cases are confirmed. The next step will be to investigate the role of chain flexibility on the coil-stretch transition and on tumbling dynamics. The model for the dynamics of these chains will also be extended to include the effect of hydrodynamic interactions between beads (as in [40]). Another question remains to be explored:

What is happening when fluctuations are triggered by the flow itself rather than by noise? This issue will be investigated by coupling the dynamics of such chains with turbulent velocity gradients (coming directly from direct numerical simulations). The role of fluctuations both in the intensity of the velocity gradient and in its direction will be explored. In the general context of flexible particles in turbulent flows, further studies are needed to evaluate the effect of preferential sampling and preferential concentration of such fibers in the near-wall region, especially in the case of highly elongated and deformable fibers. Future studies will also explore the dynamics of chains with a size longer than the smallest scale of variation of the fluid velocity field: in that case, the velocity gradient along the chain will not be constant but governed by the turbulent flow. Since fluctuations due to turbulence do have spatial and temporal correlations, we expect complex behavior of such chains that can be very different from that obtained in the present study (where a white noise has been used for thermal fluctuations). These issues will be probed in future studies by coupling the dynamics of such fibers with direct simulations of wall-bounded turbulent flows.

## ACKNOWLEDGMENTS

This work has been supported by the French government, through the Investments for the Future project UCA$^{\text{JEDI}}$ managed by the National Research Agency (ANR) with the reference number ANR-15-IDEX-01. The work of C.H. was supported by the PRESTIGE Program (Grant No. PRESTIGE-2017-1-0025) coordinated by Campus France. Through this PRESTIGE program, this research has received funding from the People Program (Marie Curie Actions) of the European Union's Seventh Framework Program (FP7/2007-2013) under REA Grant Agreement No. PCOFUND-GA-2013-609102. C.H. acknowledges the support of the EU COST Action MP1305 "Flowing Matter." The authors acknowledge Dario Vincenzi for fruitful discussions. The authors thank the reviewers for their insightful comments and suggestions.

## APPENDIX

### 1. Implementation in the general case

In the following, we focus on the numerical implementation of the chain equation of motion in an extensional flow. In that case, it is given by Eq. (4) which can be rewritten as

$$\frac{d\boldsymbol{\xi}_i}{dt} = \boldsymbol{V}_i, \tag{A1}$$

$$\frac{d\boldsymbol{V}_i}{dt} = -\frac{\zeta}{m}[\boldsymbol{V}_i - \boldsymbol{\xi}_i \cdot \boldsymbol{\nabla u}] + \sqrt{\frac{2k_{\mathrm{B}}T\zeta}{m^2\ell_{\mathrm{K}}^2}}\,(\boldsymbol{\eta}_i - \boldsymbol{\eta}_{i-1}) + 2\lambda_i\boldsymbol{\xi}_i - \lambda_{i+1}\boldsymbol{\xi}_{i+1} - \lambda_{i-1}\boldsymbol{\xi}_{i-1}. \tag{A2}$$

This equation is solved using a simple first-order Euler-Maruyama method with temporal discretization (time step $\Delta t$):

$$\boldsymbol{V}_i(t+\Delta t) = \boldsymbol{V}_i(t) + \delta\boldsymbol{V}_i(t),$$
$$\boldsymbol{\xi}_i(t+\Delta t) = \boldsymbol{\xi}_i(t) + \Delta t\,\boldsymbol{V}_i(t) \tag{A3}$$

with the variation of the bead velocity given by

$$\delta\boldsymbol{V}_i(t) = -\Delta t\frac{\zeta}{m}[\boldsymbol{V}_i(t) - \boldsymbol{\xi}_i(t)\cdot\boldsymbol{\nabla u}] + \sqrt{\Delta t}K_{\mathrm{Br}}(\boldsymbol{\gamma}_i - \boldsymbol{\gamma}_{i-1}) - \Delta t\,(\Delta_\xi\boldsymbol{\lambda})_i \tag{A4}$$

with $K_{\mathrm{Br}} = \sqrt{2k_{\mathrm{B}}T\zeta}/(m\ell_{\mathrm{K}})$ the diffusion coefficient for Brownian motion, $\gamma_i$ taken from a Gaussian distribution (with zero mean and a standard deviation equal to 1), $\boldsymbol{\lambda}$ denotes the $N$-dimensional vector $(\lambda_1,\ldots,\lambda_N)^{\mathsf{T}}$, and $\boldsymbol{\Delta}_\xi$ is such that $(\boldsymbol{\Delta}_\xi\boldsymbol{\lambda})_i = -2\lambda_i\boldsymbol{\xi}_i + \lambda_{i-1}\boldsymbol{\xi}_{i-1} + \lambda_{i+1}\boldsymbol{\xi}_{i+1}$.

The tension forces acting on each rigid segment is obtained by imposing a constant distance between consecutive beads $|\boldsymbol{\xi}_i(t+\Delta t)|^2 = |\boldsymbol{\xi}_i(t)|^2$ for all $1 \leqslant i \leqslant N$. Using Eq. (A3), this leads to

$$2\boldsymbol{\xi}_i(t)\cdot\boldsymbol{V}_i(t) + \Delta t|\boldsymbol{V}_i(t)|^2 = 0. \tag{A5}$$

By writing the above equation at time $t+\Delta t$, we obtain

$$2\Delta t\,|\boldsymbol{V}_i(t)|^2 + 2\boldsymbol{\xi}_i(t)\cdot\delta\boldsymbol{V}_i(t) + 4\Delta t\boldsymbol{V}_i(t)\cdot\delta\boldsymbol{V}_i(t) + \Delta t|\delta\boldsymbol{V}_i(t)|^2 = 0. \tag{A6}$$

The above nonlinearities do not allow for writing an explicit solution. Yet, one can note that the terms on the left-hand side involve various powers of the time step $\Delta t$. For that reason, we chose to decompose the tensions $\lambda_i$ as series in powers of $\sqrt{\Delta t}$, i.e.,

$$\Delta t\boldsymbol{\lambda} = \sum_{k=1}^{\infty}\boldsymbol{\lambda}^{(k)}\Delta t^{k/2}. \tag{A7}$$

The series starts with terms $O(\sqrt{\Delta t})$ to account for the tension that balances the noise. We can then identify each contribution to obtain a set of equations for each term:

(1) Terms in $\Delta t^{1/2}$:

$$\boldsymbol{\xi}_i\cdot(\boldsymbol{\Delta}_\xi\boldsymbol{\lambda}^{(1)})_i = K_{\mathrm{Br}}\boldsymbol{\xi}_i\cdot(\boldsymbol{\gamma}_i - \boldsymbol{\gamma}_{i-1}).$$

(2) Terms in $\Delta t$:

$$\boldsymbol{\xi}_i\cdot(\boldsymbol{\Delta}_\xi\boldsymbol{\lambda}^{(2)})_i = |\boldsymbol{V}_i|^2 - \frac{\zeta}{m}\boldsymbol{\xi}_i\cdot(\boldsymbol{V}_i - \boldsymbol{\xi}_i\cdot\boldsymbol{\nabla u}).$$

(3) Terms in $\Delta t^{3/2}$:

$$\boldsymbol{\xi}_i\cdot(\boldsymbol{\Delta}_\xi\boldsymbol{\lambda}^{(3)})_i = 2\boldsymbol{V}_i\cdot[K_{\mathrm{Br}}(\boldsymbol{\gamma}_i - \boldsymbol{\gamma}_{i-1}) - (\boldsymbol{\Delta}_\xi\boldsymbol{\lambda}^{(1)})_i].$$

(4) Terms in $\Delta t^2$:

$$\boldsymbol{\xi}_i\cdot(\boldsymbol{\Delta}_\xi\boldsymbol{\lambda}^{(4)})_i = 2\boldsymbol{V}_i\cdot\left[-\frac{\zeta}{m}\boldsymbol{\xi}_i\cdot(\boldsymbol{V}_i - \boldsymbol{\xi}_i\cdot\boldsymbol{\nabla u}) - (\boldsymbol{\Delta}_\xi\boldsymbol{\lambda}^{(2)})_i\right] + \frac{1}{2}|K_{\mathrm{Br}}(\boldsymbol{\gamma}_i - \boldsymbol{\gamma}_{i-1}) - (\boldsymbol{\Delta}_\xi\boldsymbol{\lambda}^{(1)})_i|^2.$$

The above expansion can be continued to reach an arbitrary precision. In practice, we stop at a given order and use the corresponding approximation of the tensions to update the chain velocity. In the paper, we used the expansion to order $\Delta t$. The terms order $\Delta t^{3/2}$ are stochastic with a zero mean, so that the error is on average $O(\Delta t^2)$.

### 2. Implementation for small chains

In the case of chains composed of beads that act as tracers in the flow, the equation of motion simplifies to

$$\frac{d\boldsymbol{\xi}_i}{dt} = \boldsymbol{\xi}_i \cdot \boldsymbol{\nabla u} + \sqrt{\frac{2k_B T}{\ell_K^2 \zeta}}(\boldsymbol{\eta}_i - \boldsymbol{\eta}_{i-1}) + 2\lambda_i' \boldsymbol{\xi}_i - \lambda_{i+1}' \boldsymbol{\xi}_{i+1} - \lambda_{i-1}' \boldsymbol{\xi}_{i-1}, \tag{A8}$$

with $\lambda' = \lambda m/\zeta$. This equation is solved using a first-order Euler-Maruyama method with time step $\Delta t$:

$$\boldsymbol{\xi}_i(t + \Delta t) = \boldsymbol{\xi}_i(t) + \delta\boldsymbol{\xi}_i(t) \tag{A9}$$

with the variation of the bead position $\delta\boldsymbol{\xi}_i(t)$ given by

$$\delta\boldsymbol{\xi}_i(t) = \Delta t\, \boldsymbol{\xi}_i(t) \cdot \boldsymbol{\nabla u} + \sqrt{\Delta t} K_{Br}'(\boldsymbol{\gamma}_i - \boldsymbol{\gamma}_{i-1}) - \Delta t(\Delta_\xi \boldsymbol{\lambda}')_i \tag{A10}$$

with $K_{Br}' = \sqrt{(2k_B T)/(\zeta \ell_K^2)}$ the diffusion coefficient for Brownian motion, the $\gamma_i$'s taken from a Gaussian distribution (with zero mean and a standard deviation 1).

The tension forces acting on each rigid segment are obtained by imposing a constant distance between consecutive beads, i.e., $|\boldsymbol{\xi}_i(t + \Delta t)|^2 = |\boldsymbol{\xi}_i(t)|^2$, leading to

$$2\boldsymbol{\xi}_i(t) \cdot \delta\boldsymbol{\xi}_i(t) + |\delta\boldsymbol{\xi}_i(t)|^2 = 0. \tag{A11}$$

As in the inertial case, we decompose the tensions $\lambda_i'$ as

$$\Delta t \boldsymbol{\lambda}' = \sum_{k=1}^{\infty} \boldsymbol{\lambda}'^{(k)} \Delta t^{k/2}, \tag{A12}$$

and identify contributions of different orders in $\Delta t^{1/2}$:

(1) Terms in $\Delta t^{1/2}$:

$$\boldsymbol{\xi}_i \cdot (\Delta_\xi \boldsymbol{\lambda}'^{(1)})_i = K_{Br}' \boldsymbol{\xi}_i \cdot (\boldsymbol{\gamma}_i - \boldsymbol{\gamma}_{i-1}).$$

(2) Terms in $\Delta t$:

$$\boldsymbol{\xi}_i \cdot (\Delta_\xi \boldsymbol{\lambda}'^{(2)})_i = \boldsymbol{\xi}_i \cdot (\boldsymbol{\xi}_i \cdot \boldsymbol{\nabla u}) - K_{Br}'(\boldsymbol{\gamma}_i - \boldsymbol{\gamma}_{i-1}) \cdot (\Delta_\xi \boldsymbol{\lambda}'^{(1)})_i + \tfrac{1}{2}|K_{Br}'(\boldsymbol{\gamma}_i - \boldsymbol{\gamma}_{i-1})|^2 + \tfrac{1}{2}|(\Delta_\xi \boldsymbol{\lambda}'^{(1)})_i|^2.$$

(3) Terms in $\Delta t^{3/2}$ :

$$\boldsymbol{\xi}_i \cdot (\Delta_\xi \boldsymbol{\lambda}'^{(3)})_i = [\boldsymbol{\xi}_i \cdot \boldsymbol{\nabla u} - (\Delta_\xi \boldsymbol{\lambda}'^{(2)})_i] \cdot [K_{Br}'(\boldsymbol{\gamma}_i - \boldsymbol{\gamma}_{i-1}) - (\Delta_\xi \boldsymbol{\lambda}'^{(1)})_i].$$

(4) Terms in $\Delta t^2$:

$$\boldsymbol{\xi}_i \cdot (\Delta_\xi \boldsymbol{\lambda}'^{(4)})_i = -(\boldsymbol{\xi}_i \cdot \boldsymbol{\nabla u}) \cdot (\Delta_\xi \boldsymbol{\lambda}'^{(2)})_i \times [(\Delta_\xi \boldsymbol{\lambda}'^{(1)})_i - K_{Br}'(\boldsymbol{\gamma}_i - \boldsymbol{\gamma}_{i-1})] \cdot (\Delta_\xi \boldsymbol{\lambda}'^{(3)})_i + \tfrac{1}{2}|\boldsymbol{\xi}_i \cdot \boldsymbol{\nabla u}|^2 + \tfrac{1}{2}|(\Delta_\xi \boldsymbol{\lambda}'^{(2)})_i|^2.$$

The above approximation, with terms up to those of order $\Delta t^2$, is used in the paper.


[1] F. Lundell, L. D. Söderberg, and P. H. Alfredsson, Annu. Rev. Fluid Mech. **43**, 195 (2011).
[2] H. Cui and J. R. Grace, Int. J. Multiphase Flow **33**, 921 (2007).
[3] E. S. Shaqfeh, J. Non-Newtonian Fluid Mech. **130**, 1 (2005).
[4] P.-G. De Genne, *Introduction to Polymer Dynamics* (Cambridge University Press, Cambridge, 1990).
[5] K. Binder, J. Baschnagel, and W. Paul, Prog. Polym. Sci. **28**, 115 (2003).
[6] T. Sridhar, D. A. Nguyen, R. Prabhakar, and J. R. Prakash, Phys. Rev. Lett. **98**, 167801 (2007).
[7] P. A. Jumars, J. H. Trowbridge, E. Boss, and L. Karp-Boss, Marine Ecology **30**, 133 (2009).
[8] H. R. Pruppacher, J. D. Klett, and P. K. Wang, Aerosol. Sci. Technol. **28**, 381 (1998).
[9] A. Lindner and M. Shelley, *Fluid-Structure Interactions in Low-Reynolds-Number Flows* (Royal Society of Chemistry, London, 2015), Vol. 168, pp. 168–192.
[10] C. Brouzet, G. Verhille, and P. Le Gal, Phys. Rev. Lett. **112**, 074501 (2014).
[11] T. T. Perkins, D. E. Smith, and S. Chu, Science **264**, 819 (1994).
[12] T. T. Perkins, D. E. Smith, R. G. Larson, and S. Chu, Science **268**, 83 (1995).
[13] G. Verhille and A. Bartoli, Exp. Fluids **57**, 1 (2016).
[14] V. Kantsler and R. E. Goldstein, Phys. Rev. Lett. **108**, 038103 (2012).
[15] K.-W. Hsiao, C. Sasmal, J. Ravi Prakash, and C. M. Schroeder, J. Rheol. **61**, 151 (2017).
[16] M. Harasim, B. Wunderlich, O. Peleg, M. Kröger, and A. R. Bausch, Phys. Rev. Lett. **110**, 108302 (2013).
[17] Y. Liu and V. Steinberg, (Europhys Lett. **90**, 44005 (2010).
[18] M. Chertkov, Phys. Rev. Lett. **84**, 4761 (2000).
[19] H. López, J.-P. Hulin, H. Auradou, and M. D'Angelo, Phys. Fluids **27**, 013102 (2015).
[20] N. Strelnikova, M. Göllner, and T. Pfohl, Macromol. Chem. Phys. **218**, 1600474 (2017).
[21] C. Cruz, F. Chinesta, and G. Regnier, Arch. Comput. Methods Eng. **19**, 227 (2012).
[22] R. G. Larson, J. Rheol. **49**, 1 (2005).
[23] P. T. Underhill and P. S. Doyle, J. Non-Newtonian Fluid Mech. **122**, 3 (2004).
[24] O. Kratky and G. Porod, Recl. Trav. Chim. **68**, 1106 (1949).
[25] E. L. C. V. M. Plan and D. Vincenzi, in Proc. R. Soc., A **472**, 20160226 (2016).
[26] V. A. Beck and E. S. Shaqfeh, J. Rheol. **51**, 561 (2007).
[27] H. Kramers, Physica **11**, 1 (1944).
[28] M. Somasi, B. Khomami, N. J. Woo, J. S. Hur, and E. S. Shaqfeh, J. Non-Newtonian Fluid Mech. **108**, 227 (2002).
[29] P. E. Rouse, Jr., J. Chem. Phys. **21**, 1272 (1953).
[30] P. De Genne, J. Chem. Phys. **60**, 5030 (1974).
[31] A. Ali, E. L. C. V. M. Plan, S. S. Ray, and D. Vincenzi, Phys. Rev. Fluids **1**, 082402 (2016).
[32] J. S. Hur, E. S. Shaqfeh, and R. G. Larson, J. Rheol. **44**, 713 (2000).
[33] T. Watanabe and T. Gotoh, Phys. Rev. E **81**, 066301 (2010).

[34] Y.-N. Young and M. J. Shelley, Phys. Rev. Lett. **99**, 058303 (2007).
[35] J. Einarsson, B. Mihiretie, A. Laas, S. Ankardal, J. Angilella, D. Hanstorp, and B. Mehlig, Phys. Fluids **28**, 013302 (2016).
[36] S. Gerashchenko and V. Steinberg, Phys. Rev. Lett. **96**, 038304 (2006).
[37] K. Gustavsson, J. Einarsson, and B. Mehlig, Phys. Rev. Lett. **112**, 014501 (2014).
[38] K. Turitsyn, J. Exp. Theor. Phys. **105**, 655 (2017).
[39] T. T. Perkins, D. E. Smith, and S. Chu, Science **276**, 2016 (1997).
[40] C.-C. Hsieh, L. Li, and R. G. Larson, J. Non-Newtonian Fluid Mech. **113**, 147 (2003).